NATIONAL TRANSPORTATION SAFETY BOARD

Office of Research and Engineering
Materials Laboratory Division
Washington, D.C. 20594

January 3, 2022

MATERIALS LABORATORY STUDY   Report No. 21-092

A. ACCIDENT INFORMATION

Place	:	Daytona Beach, Florida
Date	:	April 4, 2018
Vehicle	:	Piper PA-28R-201, N106ER
NTSB No.	:	ERA18FA120
Investigator	:	Aaron McCarter, AS-ERA / Clinton R. Crookshanks, AS-40

B. COMPONENTS EXAMINED

2 exemplar left wing main spar lower spar cap pieces with fatigue cracks.
Spar A: removed from a Piper PA-28RT-201T, S/N 28R-7931247
Spar B: removed from a Piper PA-28R-201, S/N 2844098

C. DETAILS OF THE STUDY

Three exemplar wing spar pieces from Piper airplanes were received for examination at the NTSB Materials Laboratory. As documented in Materials Laboratory Factual Report 21-091,[1] fatigue cracks were observed in two of the wing spars (denoted spar A and spar B) from the airplanes noted above. The locations of the cracks in spars A and B are shown in figure 1. This document is a study of the estimated crack growth behavior based on fracture surface observations.

Available information about the service history of the spars was relatively limited. Spar A was removed from an airplane that was manufactured in 1979. Registration records online indicate the airplane changed ownership in January 2003 from an owner in Oklahoma, United States to an owner in the United Kingdom. Pictures available online indicate the airplane was repainted sometime between August 25, 2017 and June 24, 2018. Another picture online showed the airplane without a propeller installed while parked outside in the United Kingdom at Perth airport on October 11, 2020. An ad was found online on December 11, 2021, indicating the airplane had been recently sold. The ad stated the airplane was up to date on its annual inspections until April 2022 and had 5,959 hours on the airframe.

Spar B was removed from an airplane that was manufactured in 2003. A review of registrations records indicated that after a brief ownership by a corporation from Salt Lake City, Utah, the airplane was owned by a limited liability company (LLC) based in

---

[1] M. R. Fox, Accident Docket ERA18FA120, Materials Laboratory Factual Report 21-091, National Transportation Safety Board (2022).

Scottsdale, Arizona from 2003 to 2008. The airplane was then owned by Embry-Riddle Aeronautical University (ERAU) for the next 7 years followed by a leasing company from Daytona Beach for 3.5 years. The airplane was then owned for 2 years by another LLC from Decatur, Alabama before being sold to the current owner, also an LLC, in August 2020. Accumulated time on the airframe was 9,378 hours at the time of the crack find. Based on usage patterns for the 2018 accident ERAU airplane and assuming a similar usage for the airplane with spar B, the estimated time and flight cycles accumulated when owned by ERAU was estimated to be ~4,750 hours and ~4,200 flights.

The fatigue regions in spars A and B showed evidence of striations, intermediate crack arrest lines, and relatively prominent crack arrest lines. Typically 5 to 10 striations were observed between the intermediate arrest lines. The intermediate arrest lines had a more distinct character relative to striations, often with radial features emanating from the convex side of the arrest lines particularly in later crack growth cycles. Based on the consistency, density, and spacing, the intermediate crack arrest lines are likely associated with flight cycles. Individual striations are likely associated with gust and maneuver loads including landing cycles between flight cycles. Relatively prominent crack arrest lines are optically visible features on the fracture surface that are typically associated with a change in stress state, environment, or time interval associated with fatigue crack growth. In the studied spar cracks, they were often characterized by oxidation patterns or additional radial features that increased their visibility relative to the intermediate arrest lines. In these cases, the relatively prominent crack arrest lines could be associated with changes in operating or storage conditions, extended calendar times between clusters of more frequent flights, or a high-load event such as an abnormally hard landing.

An overall view of fracture features associated with the crack in spar A is shown in figure 2. SEM images of typical fatigue features at multiple locations from the crack boundary to the origin are shown in figures 3 through 8. Many of the fracture features were damaged by oxidation and contact from hard particles that had migrated into the crack. However, relatively prominent arrest lines, intermediate arrest lines, and striations were noted on the crack surfaces as identified in figures 3 through 7. At the crack origin, radial features emanated from a pitted origin area shown bounded by a dashed line in figure 8.

The reported flight hours at the time of the crack find in spar A matched the time listed in the 2021 listing advertising the sale of the airplane. Additional recent events inferred from online photographs that could have been associated with changes in operation type or frequency included the photo of the airplane with its propeller removed in 2020 and a repaint that occurred sometime in 2017 and 2018. These recent events could be associated with relatively prominent crack arrest lines as indicated in figure 9. Several additional prominent crack arrest lines noted with unlabeled arrows in the SEM image in figure 9 could be associated with annual usage patterns assuming infrequent usage in recent years.

An overall view of fracture features associated with the crack in spar B is shown in figure 10. SEM images of typical fatigue features at multiple locations from the crack

boundary to the origin are shown in figures 11 through 17. Many of the fracture features near the origin were damaged by oxidation. However, relatively prominent arrest lines, intermediate arrest lines, and striations were noted on the crack surfaces as identified in figures 11 through 17. Fine fracture features near the origin were mostly obliterated by oxidation, but radial features and isolated areas of arrest lines emanated from an origin at the lower end of a 0.00035-inch (0.009-mm) deep corrosion pit as indicated in figure 17.

Many prominent arrest lines were observed across the fracture surface, but three were particularly distinct as shown with a dashed line and unlabeled arrows in figure 18. A distinct change in fracture plane occurred at the fatigue boundary, and the remainder of the fracture to the upper leading edge was on a slant plane consistent with overstress fracture of the final ligament between he crack tip and the surface. Another prominent arrest line near the middle of the fracture surface had a distinct step along the entire crack front with substantial radial features on the convex side indicative of substantial crack reinitiation. This crack arrest line could indicate a significant change in aircraft usage or could represent a high load event such as a hard landing. Closer to the origin, a distinct change in the oxidation pattern was associated with a prominent arrest line on the fracture surface. The distinct change in oxidation patterns suggests the prominent arrest line at that location could be associated with a change in storage environment. Based on the registration history, a change in storage environment likely occurred when the airplane was sold by ERAU or the subsequent owner from Daytona Beach, Florida.

SEM images such as those shown in figures 4 through 7 and 11 through 16 were used to study the crack growth rate. At each image location, the distance from the origin to the image center was recorded, and an image was taken at a resolution sufficient to resolve between 5 and 20 sequential arrest lines within the image frame. The arrest line density, ρ, for that image was then determined using the following equation,

$$\rho = f \frac{(n-1)}{l} \qquad\qquad \text{(Eq. 1)}$$

where n is the total number of sequential intermediate arrest lines counted in the image, l is the length from the first to last arrest line as measured on the image, and f is the magnification factor determined by dividing the measured length of the scale bar on the image by the scale bar reference length. Results of the density measurements and associated distance from the origin for cracks in spars A and B were then plotted in a chart as shown in figure 19.

The intermediate arrest line density data for spar B showed a general decreasing trend with distance from the origin consistent with changes in stress intensity under uniform cyclic loading conditions. However, the arrest line density for spar A was relatively unchanged. At the crack boundary for spar A, the arrest line density of 68 arrest lines per millimeter of crack growth was similar to that of spar B at the same distance, but contrary to expectation based on stress intensity, the arrest line density closer to the origin on Spar A was less dense with an average of 40 arrest lines per millimeter of crack growth. The observed differences in arrest line density measurements between spars A and B during early crack growth stages could be related to differences in flight profiles but

could also be due to the limited data and additional uncertainties in interpreting fracture features on spar A that stemmed from the fracture surface damage near the origin.

Next, a power-law curve with the following form was fit to the arrest line density data for spar B,

$$\rho = ax^n \tag{Eq. 2}$$

where x is the distance from the origin, and a and n are constants. Using Microsoft Excel to determine the curve fit (metric units were used for the curve fit), the constants a and n were determined to be 116.98 and -0.578, respectively. With constants determined for equation 2, the following integral was used to estimate the total number of intermediate crack arrest lines, N, associated with crack growth from the origin pit depth of 0.009 mm (0.00039 inch) to the crack boundary at 11.79 mm (0.464 inch),

$$N = \int_{0.009}^{11.79} 116.98x^{-0.578} \tag{Eq. 3}$$

By solving equation 3, the total number of intermediate arrest lines associated with crack growth from the origin pit to the crack boundary was estimated to be approximately 750. Assuming each intermediate arrest line is associated with a flight cycle, the total number of flight cycles associated with the spar B crack was estimated to be 750 cycles. Since the crack had propagated through the entire ligament forward of the attachment hole before it was opened in the lab, the number of additional flight cycles accumulated after the spar had cracked through is unknown.

By changing the upper limit of integration in equation 3 to the distance from the origin associated with an individual density measurement, the total number of accumulated flight cycles could be estimated for each measurement location. The average spacing between the intermediate arrest lines at each location was then calculated by taking the inverse of the density value. The resulting crack growth data for spar B as plotted in a log-linear chart is shown in figure 20.

Vertical dashed lines in figure 20 indicate locations of relatively prominent arrest lines including the three relatively distinct arrest lines noted in figure 18. Based on the crack growth estimate shown in figure 20, the crack had extended to the distinct oxide boundary line approximately 360 flight cycles before the crack reached the fatigue boundary, and the prominent arrest line with the distinct step had formed 220 flight cycles later (approximately 140 flight cycles before the crack reached the fatigue boundary).

Note that crack growth estimates in this study are based on available data and are subject to considerable interpretation. Additional confidence in the estimates and interpretation of the mid-level and prominent crack arrest lines could be gained through additional airplane usage data including storage conditions, typical flight profiles, and accumulated service hours for the various owners.
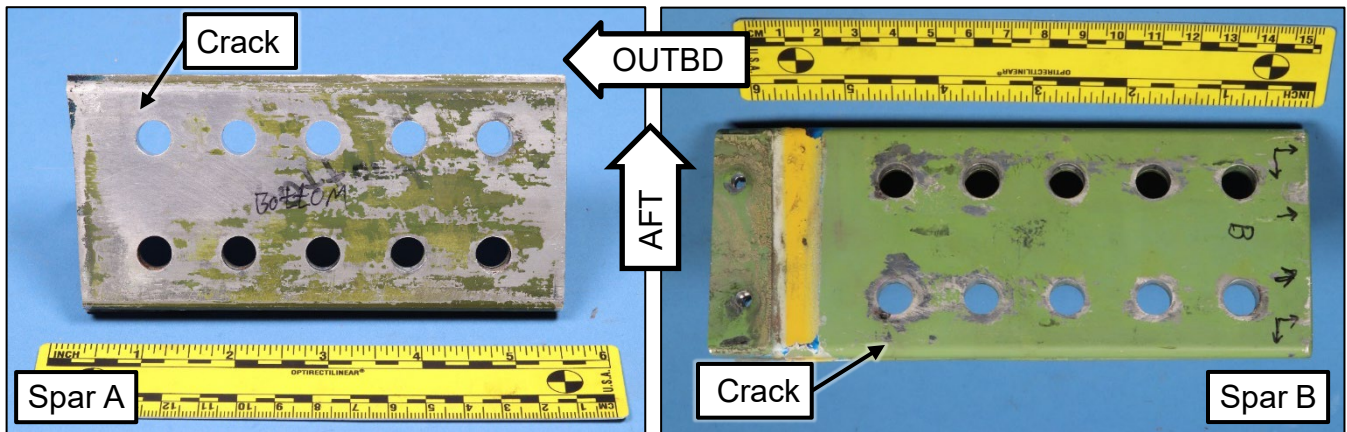

Matthew R. Fox, Ph.D.
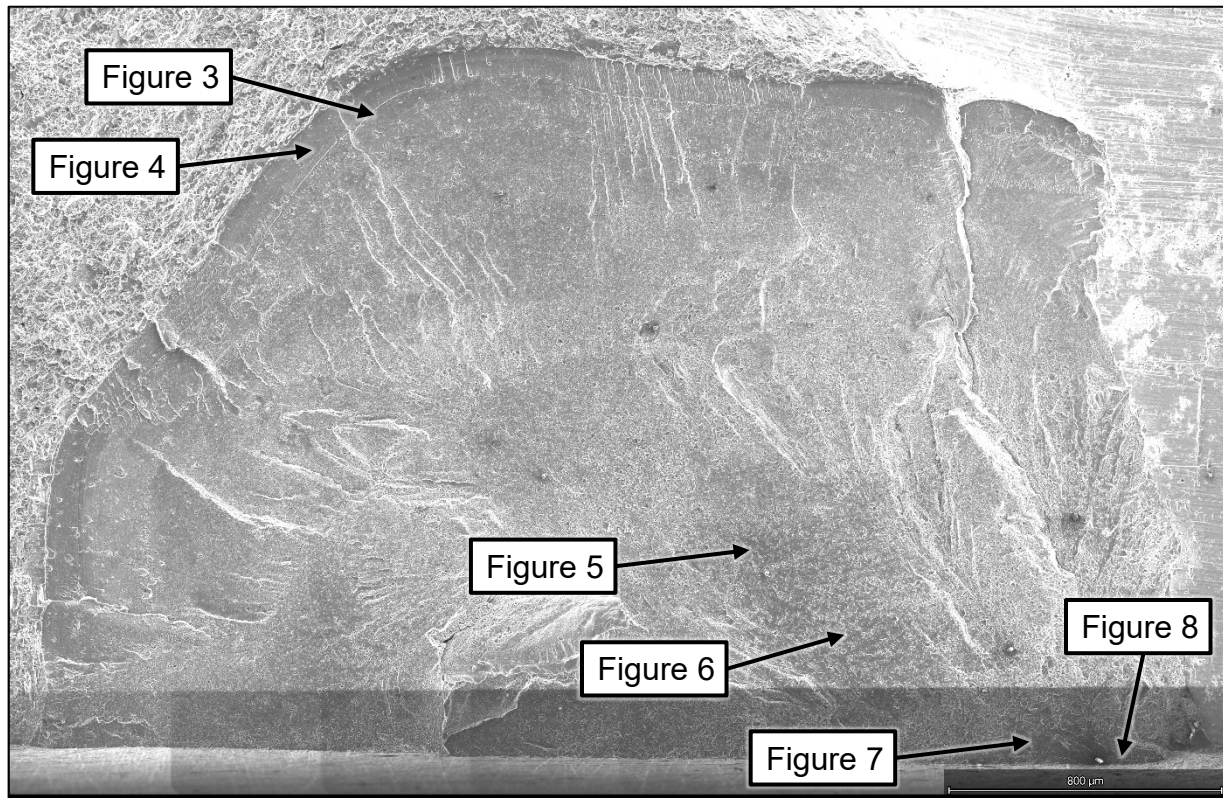Senior Materials Engineer

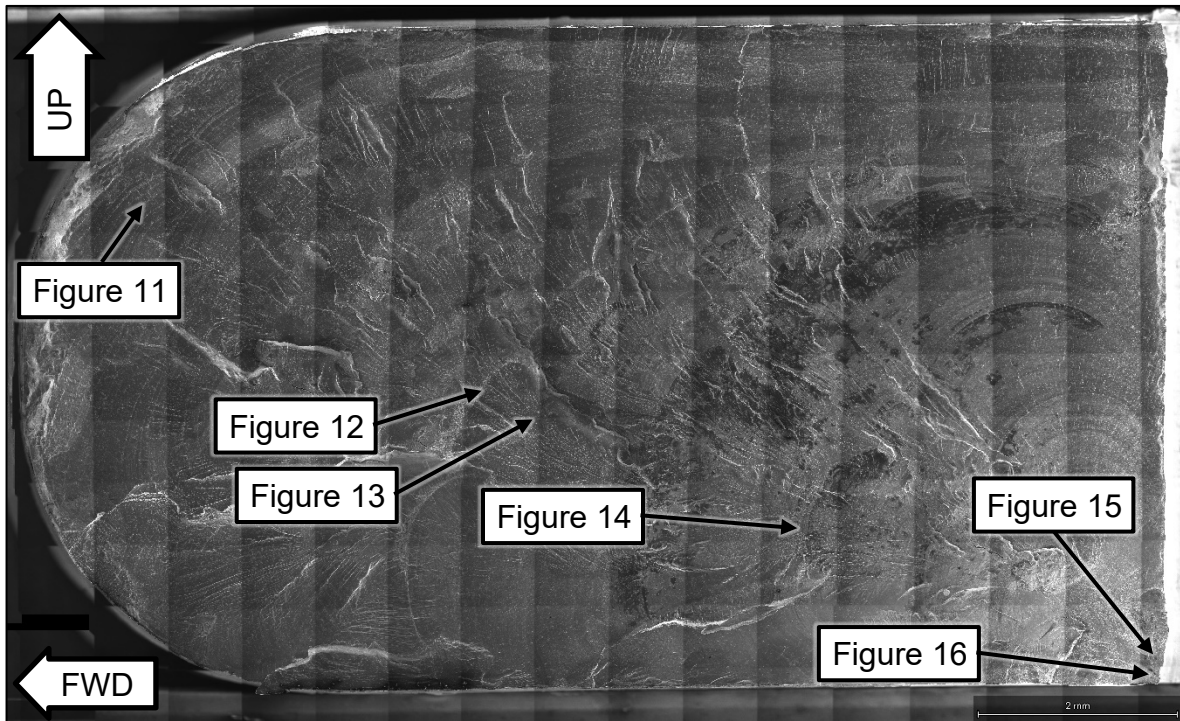Figure 1. Spars A and B lower surfaces showing crack locations.

Figure 2. Montage of SEM images showing the spar A crack fracture surface. Locations of higher magnification images shown in subsequent figures are indicated.
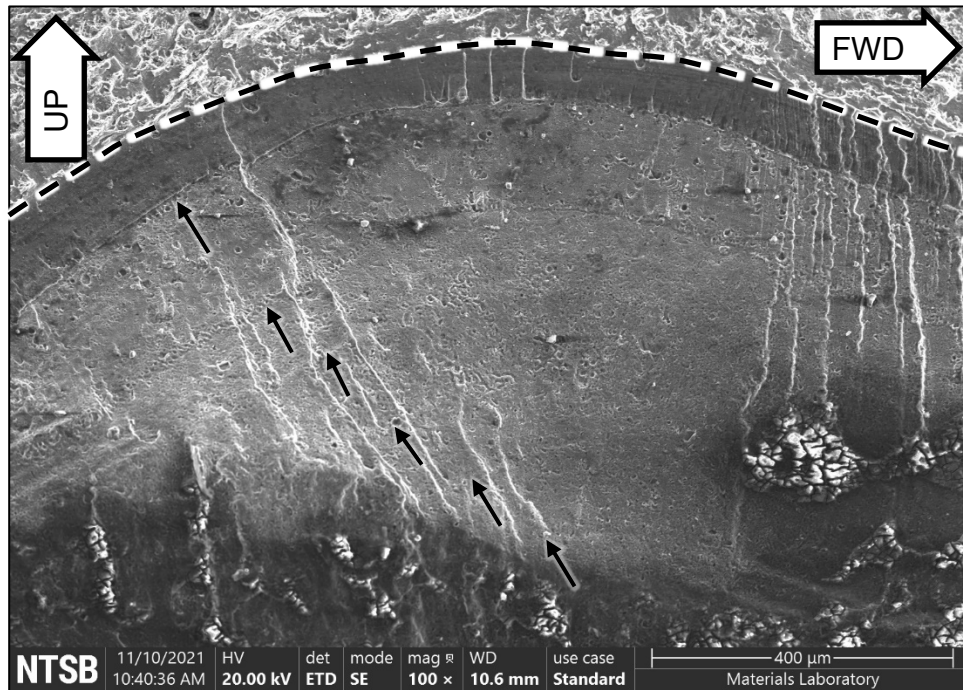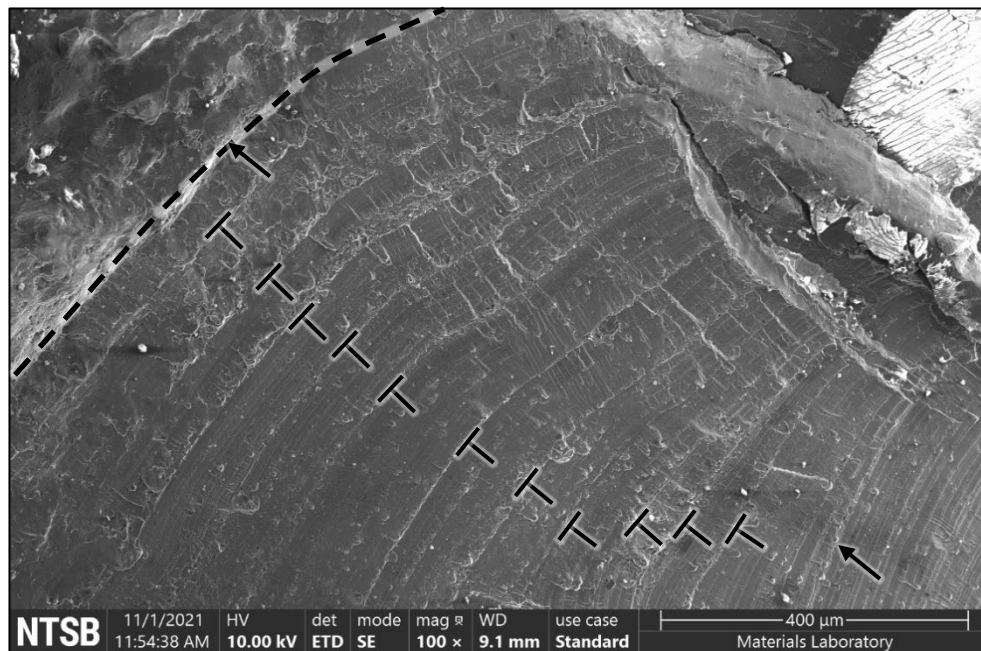
Figure 3. SEM image of the crack boundary on spar A. Unlabeled arrows indicate relatively prominent crack arrest lines, and the dashed line indicates the fatigue boundary.
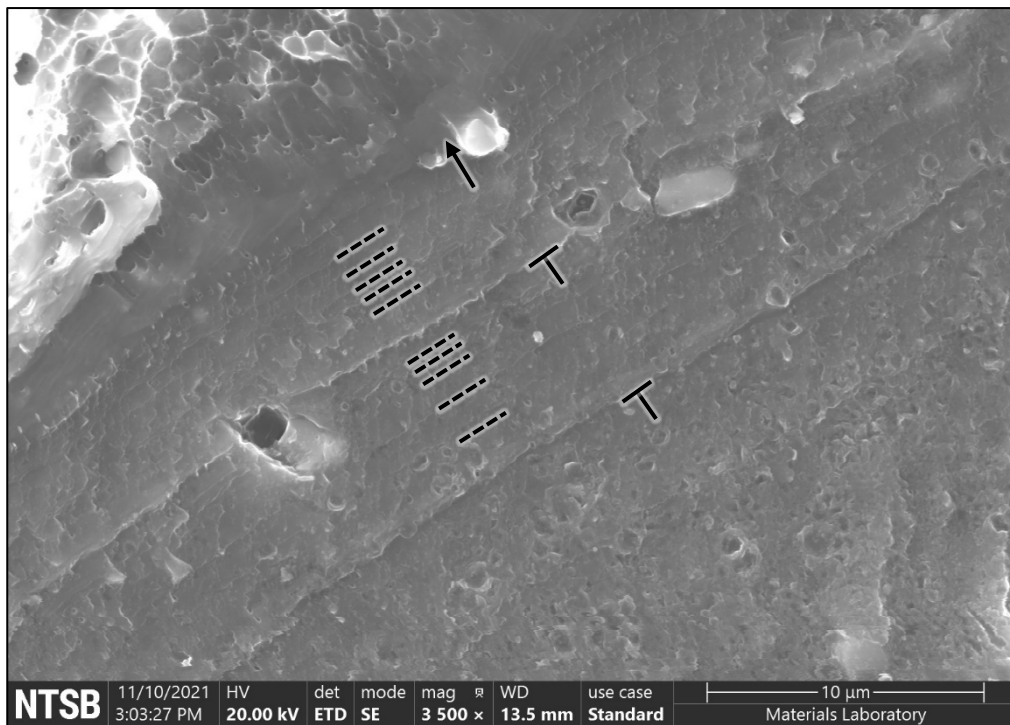
Figure 4. SEM image of the fatigue boundary located 0.116 inch (2.95 mm) from the origin on spar A. An arrow indicates the fatigue boundary, T-shaped markers indicate intermediate crack arrest lines, and dashed lines indicate striations.
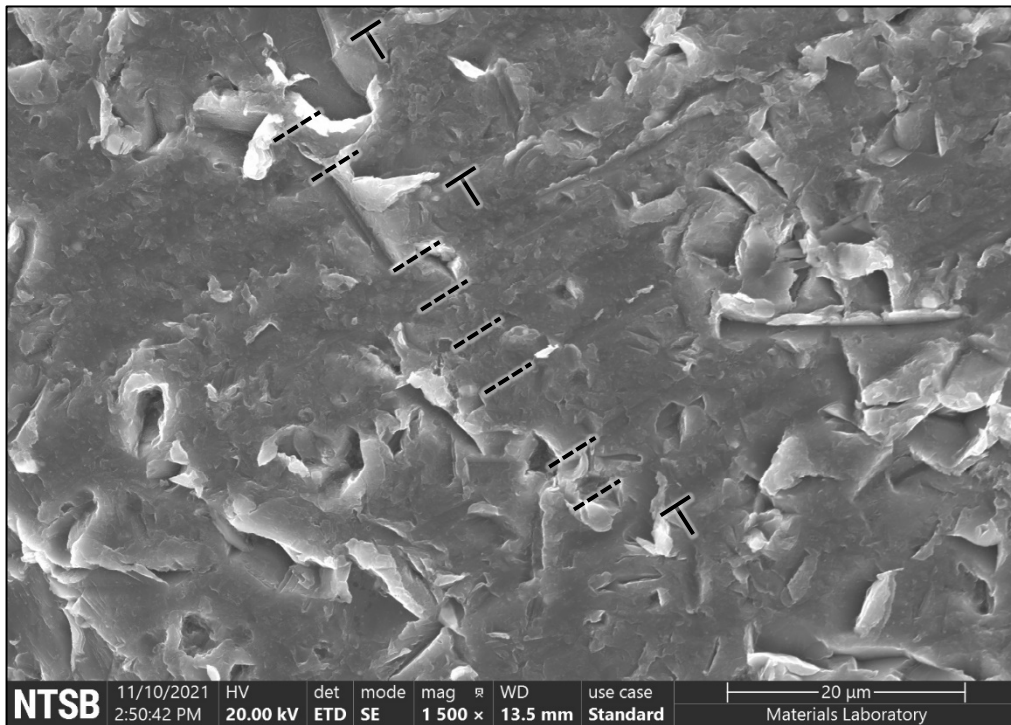
Figure 5. SEM image of fatigue features 0.0492 inch (1.25 mm) from the origin on spar A where T-shaped markers indicate intermediate crack arrest lines, and dashed lines indicate striations.
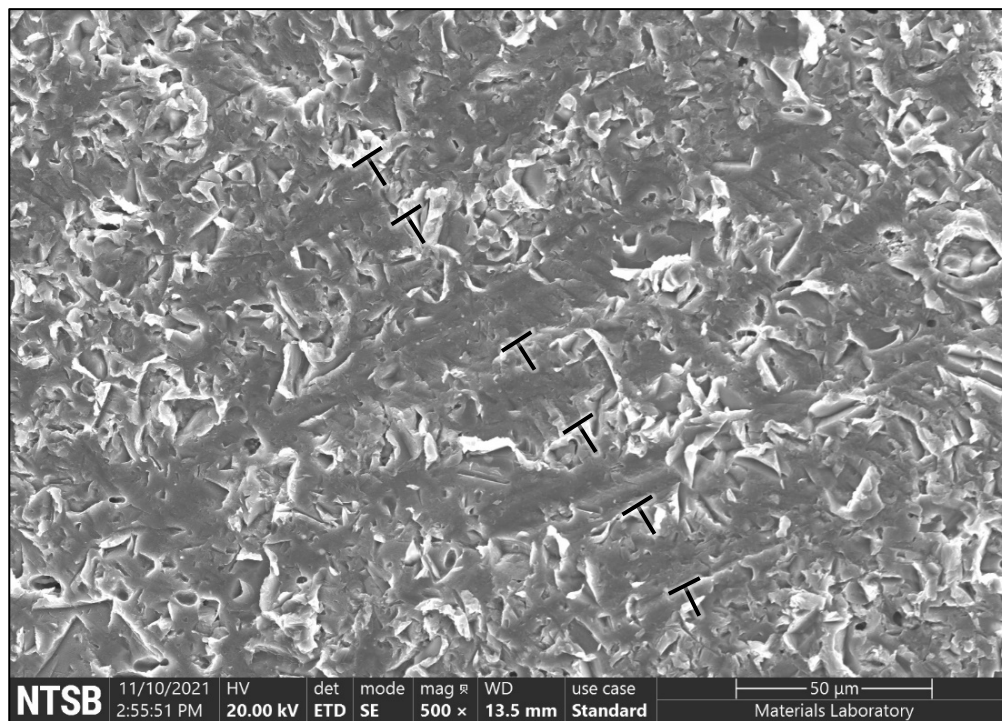
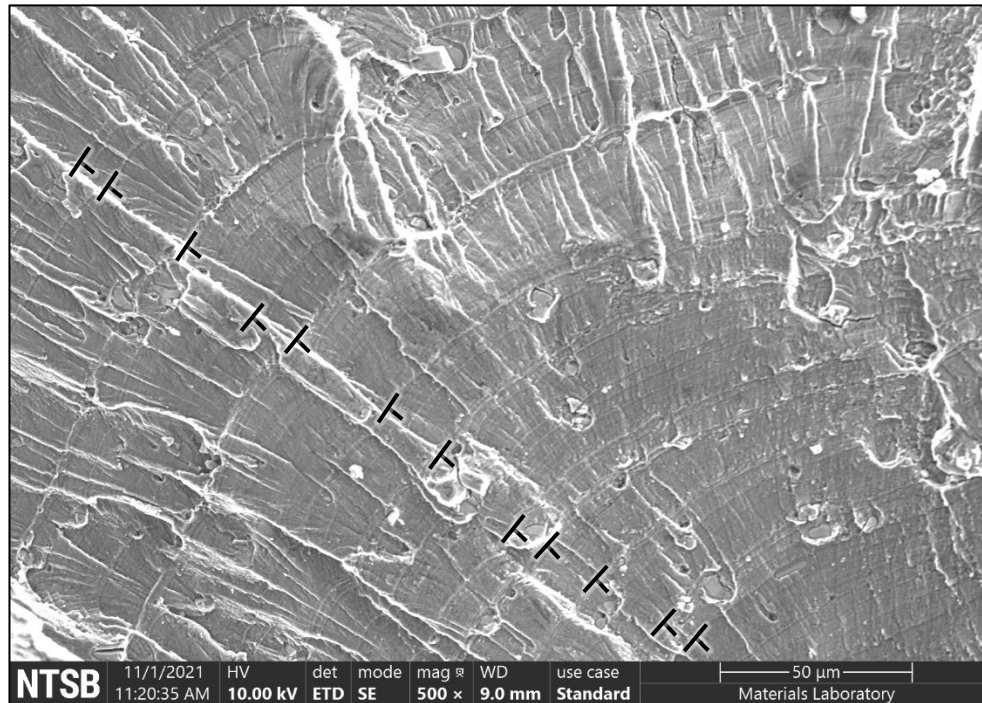Figure 6. SEM image of fatigue features 0.0328 inch (0.833 mm) from the origin on spar A showing intermediate crack arrest lines (T-shaped markers).
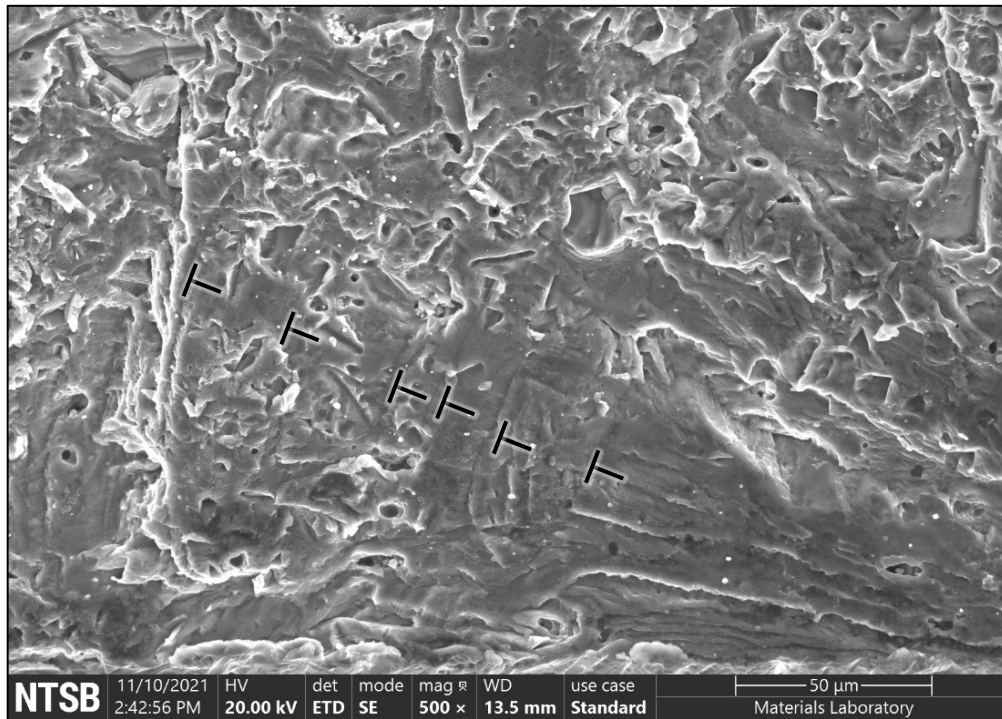
Figure 7. SEM image of fatigue features 0.0106 inch (0.269 mm) from the origin on spar A showing intermediate crack arrest lines (T-shaped markers).
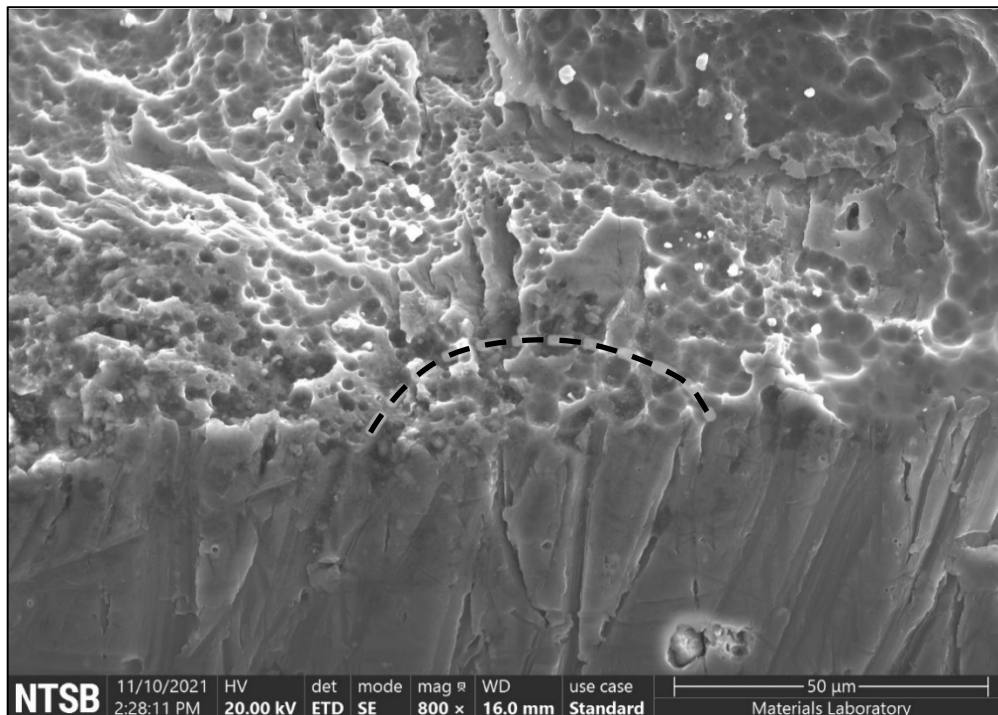

Figure 8. Spar A origin area indicated with a dashed line.
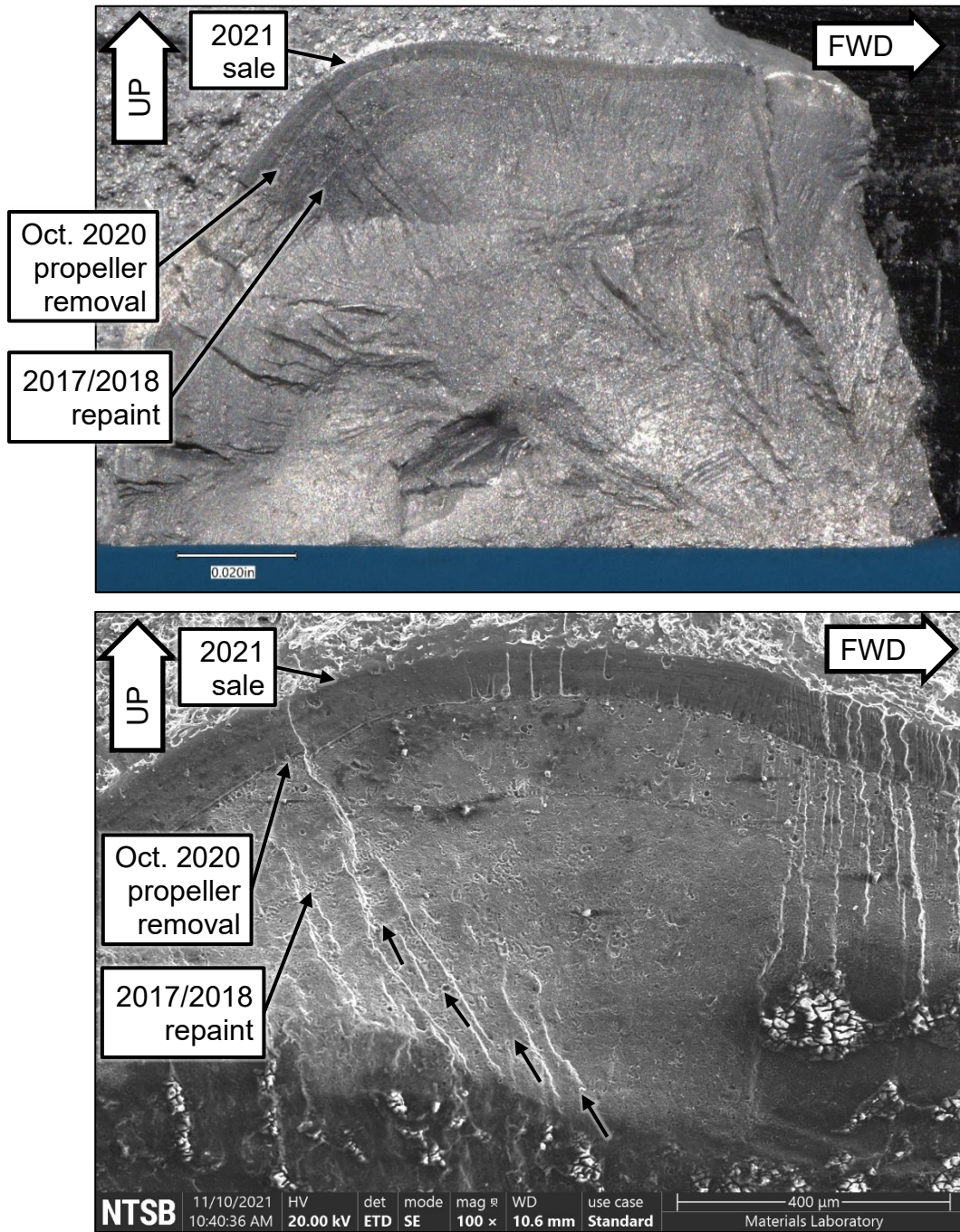
Figure 9. Optical (upper image) and SEM (lower image) images of relatively prominent arrest lines at the Spar A crack boundary with notations of possible changes in airplane usage patterns inferred from online data.

Figure 10. Montage of SEM images showing the spar B crack fracture surface. Locations of higher magnification images shown in subsequent figures are indicated.

Figure 11. SEM image of the crack boundary on spar B. Unlabeled arrows indicate relatively prominent crack arrest lines including the fatigue boundary (dashed line), and T-shaped markers indicate intermediate crack arrest lines.
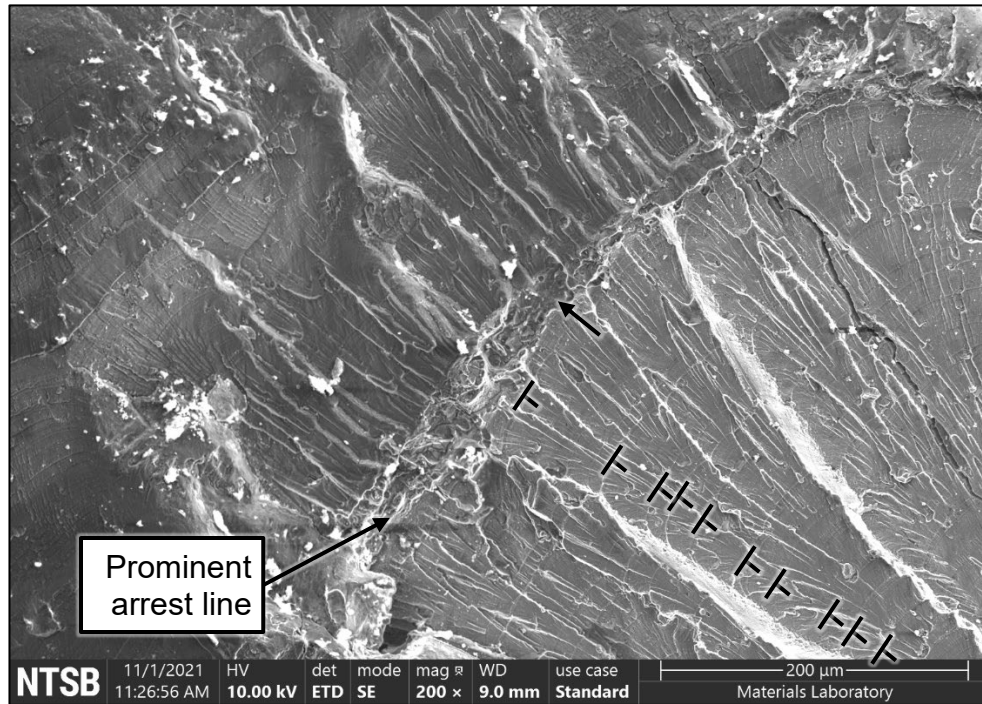
Figure 12. Prominent arrest line 0.295 inch (7.5 mm) from the origin on spar B with intermediate arrest lines indicated by T-shaped markers.

Figure 13. Fatigue features 0.274 inch (6.97 mm) from the origin on spar B showing intermediate crack arrest lines (T-shaped markers).
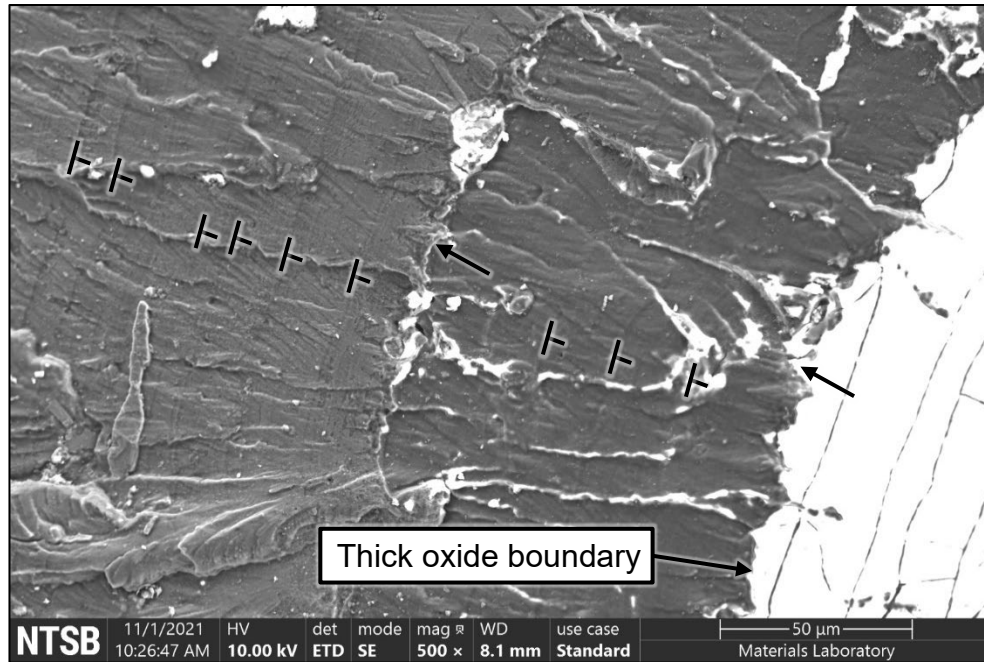
Figure 14. Fatigue features 0.114 inch (2.89 mm) from the origin on spar B showing relatively prominent crack arrest lines (unlabeled arrows) and intermediate crack arrest lines (T-shaped markers).
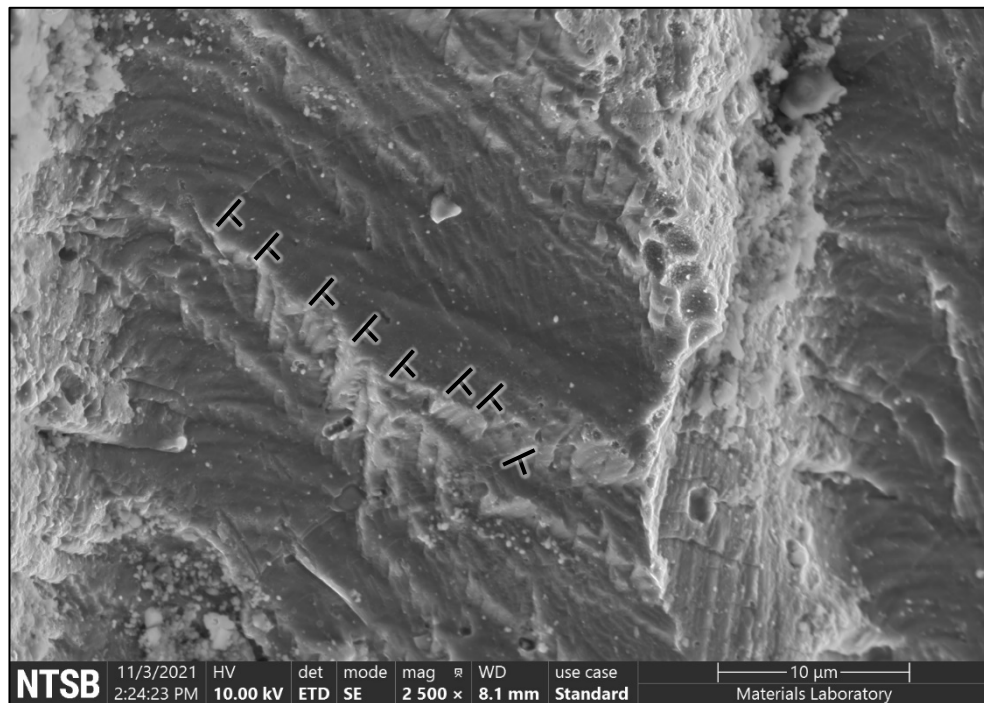

Figure 15. Fatigue features 0.0089 inch (0.226 mm) from the origin on spar B showing intermediate crack arrest lines (T-shaped markers).
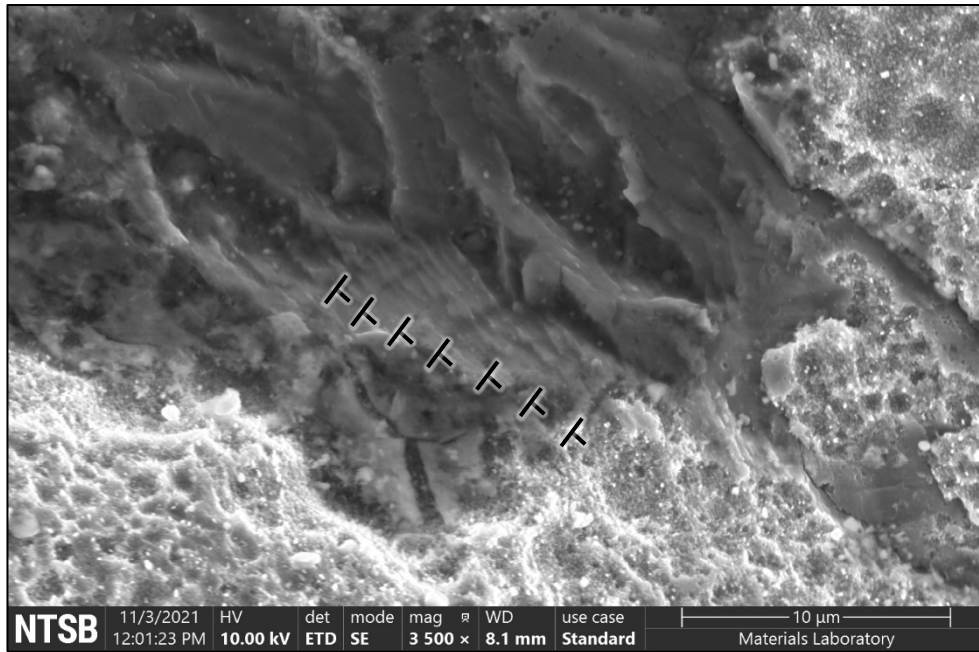
Figure 16. Fatigue features 0.0024 inch (0.062 mm) from the origin on spar B showing intermediate crack arrest lines (T-shaped markers).
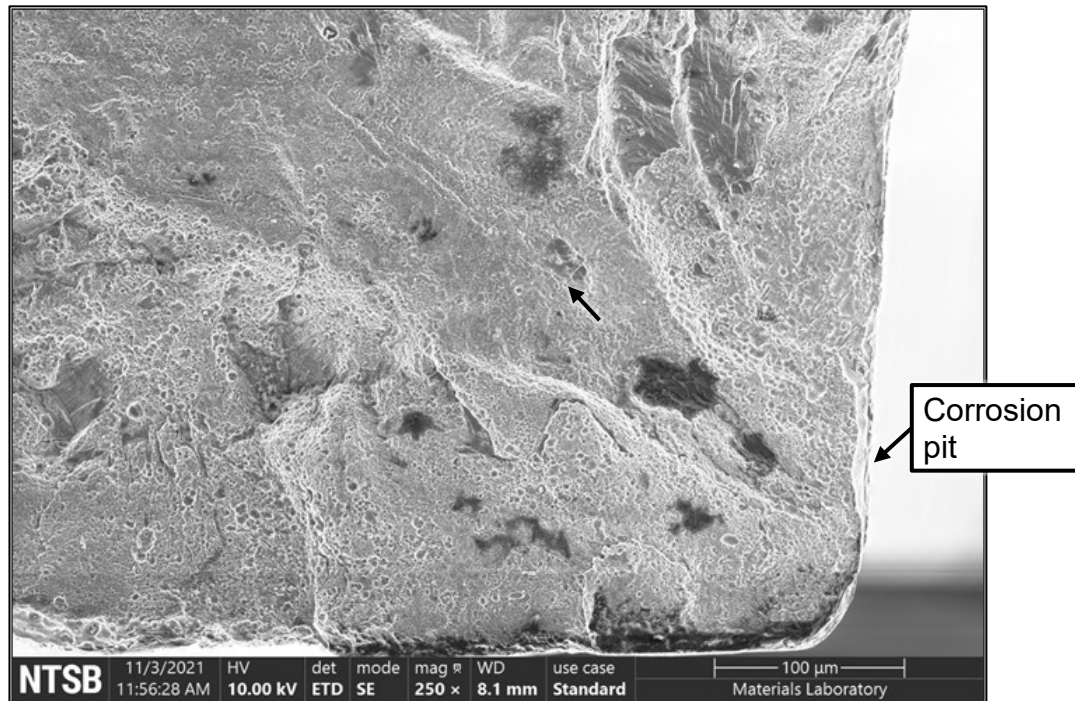

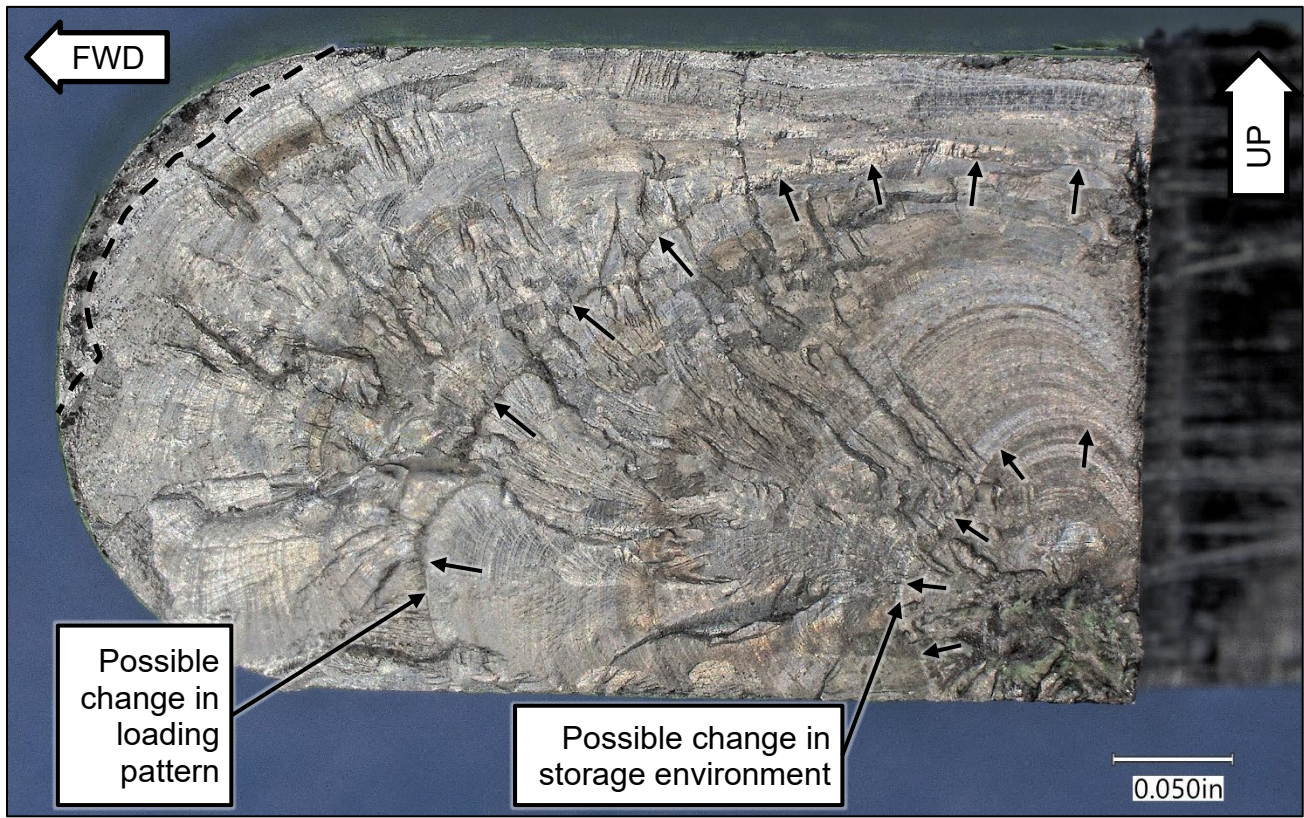Figure 17. Origin area on spar B showing a prominent arrest line near the origin (unlabeled arrow).

Figure 18. Inboard side of the fracture surface after cleaning with acetate tape and acetone. A dashed line indicates the fatigue boundary, and unlabeled arrows indicate two prominent arrest lines representing possible changes in loading pattern or environmental conditions.
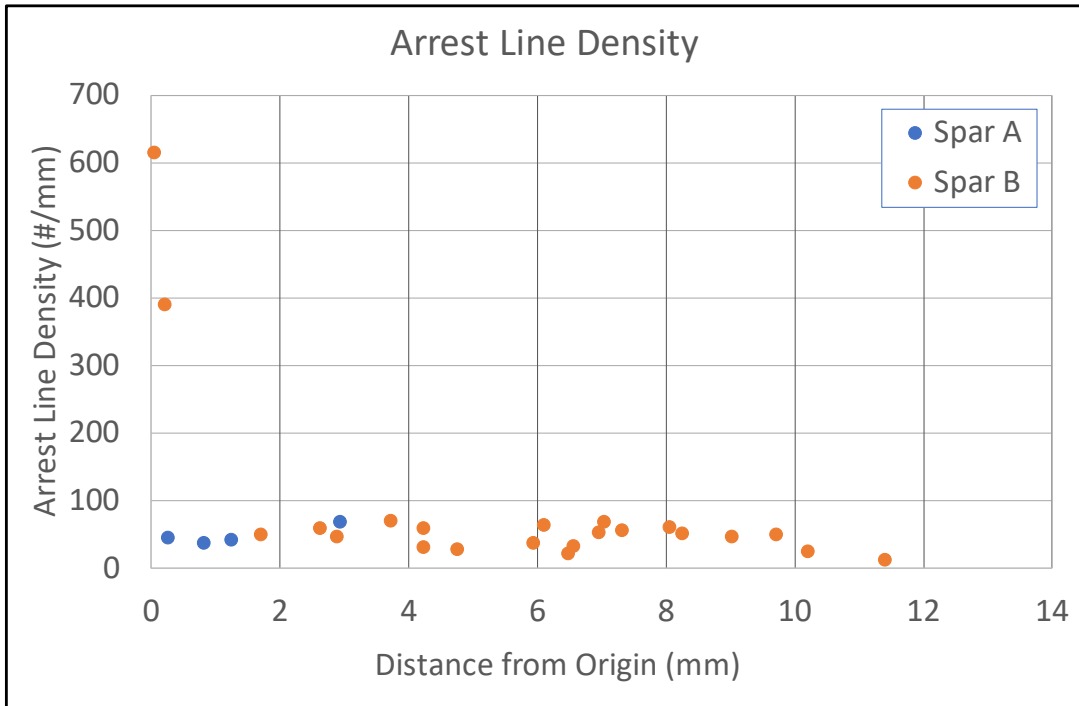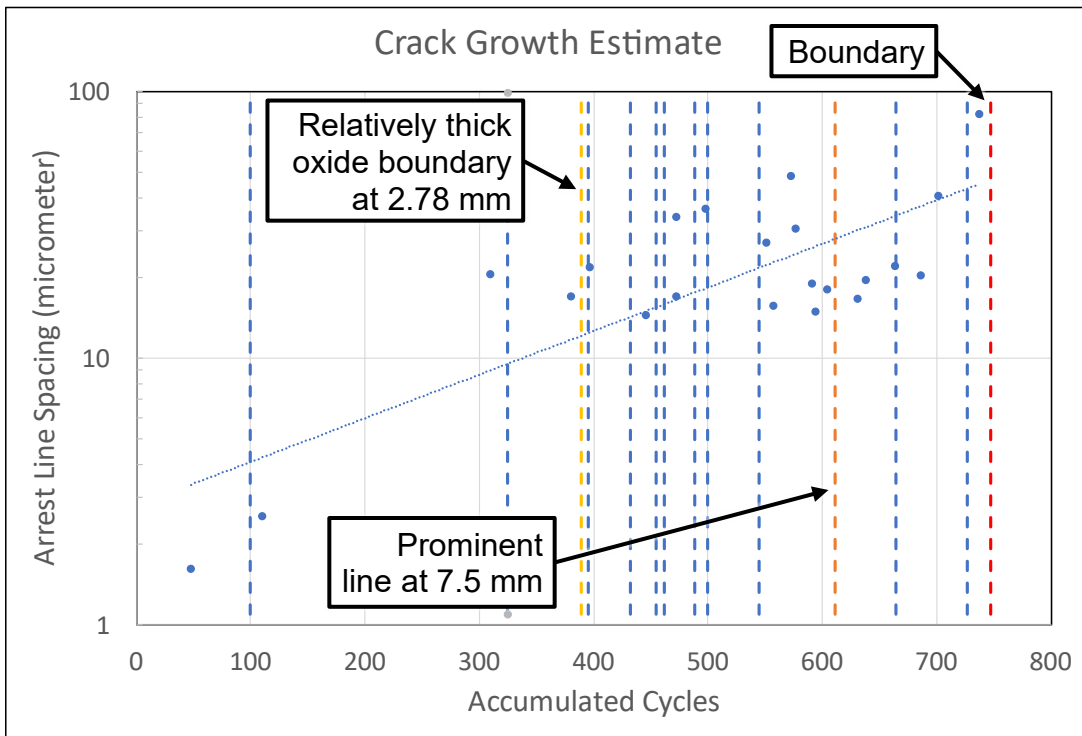
Figure 19. Arrest line density plot.

Figure 20. Crack growth estimate for spar B. Vertical dashed lines indicate relatively prominent crack arrest lines.